Applied Physics Letters

Transport properties of polarization-induced 2D electron gases in epitaxial AlScN/GaN heterojunctions

Cite as: Appl. Phys. Lett. **121**, 192101 (2022); https://doi.org/10.1063/5.0108475
Submitted: 08 July 2022 • Accepted: 15 October 2022 • Published Online: 07 November 2022

Joseph Casamento, Thai-Son Nguyen, Yongjin Cho, et al.

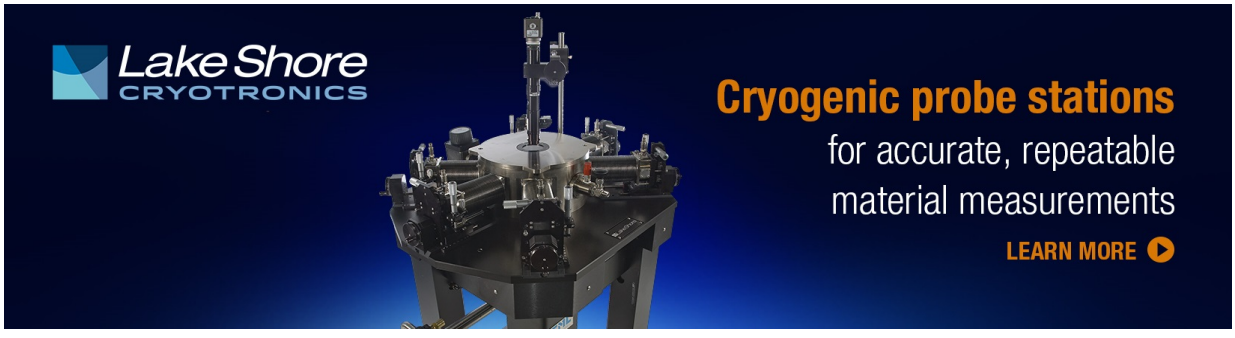

AIP Publishing

Applied Physics Letters ARTICLE scitation.org/journal/apl

Transport properties of polarization-induced 2D electron gases in epitaxial AlScN/GaN heterojunctions

Cite as: Appl. Phys. Lett. **121**, 192101 (2022); doi: 10.1063/5.0108475
Submitted: 8 July 2022 · Accepted: 15 October 2022 ·
Published Online: 7 November 2022

Joseph Casamento,[1,a)] Thai-Son Nguyen,[1] Yongjin Cho,[2] Chandrashekhar Savant,[1] Timothy Vasen,[3] Shamima Afroz,[3] Daniel Hannan,[3] Huili (Grace) Xing,[1,2,4] and Debdeep Jena[1,2,4]

AFFILIATIONS

[1]Department of Materials Science and Engineering, Cornell University, Ithaca, New York 14853, USA
[2]School of Electrical and Computer Engineering, Cornell University, Ithaca, New York 14853, USA
[3]Northrop Grumman Mission Systems Advanced Technology Laboratory, Linthicum, Maryland 21090, USA
[4]Kavli Institute at Cornell for Nanoscale Science, Cornell University, Ithaca, New York 14853, USA

[a)]**Author to whom correspondence should be addressed:** jac694@cornell.edu

ABSTRACT

AlScN is attractive as a lattice-matched epitaxial barrier layer for incorporation in GaN high electron mobility transistors due to its large dielectric constant and polarization. The transport properties of polarization-induced two-dimensional (2D) electron gas of densities of $\sim 2 \times 10^{13}/\text{cm}^2$ formed at the AlScN–GaN interface is studied by Hall-effect measurements down to cryogenic temperatures. The 2D electron gas densities exhibit mobilities limited to $\sim 300\ \text{cm}^2/\text{V s}$ down to 10 K at AlScN/GaN heterojunctions. The insertion of a ~2 nm AlN interlayer boosts the room temperature mobility by more than five times from $\sim 300\ \text{cm}^2/\text{V s}$ to $\sim 1573\ \text{cm}^2/\text{V s}$, and the 10 K mobility by more than 20 times to $\sim 6980\ \text{cm}^2/\text{V s}$ at 10 K. These measurements provide guidelines to the limits of electron conductivities of these highly polar heterostructures.

AlGaN/GaN-based nitride semiconductors have attracted significant research interest due to their application as high-electron mobility transistors (HEMTs) in high-frequency, high-power microwave, and millimeter-wave technologies.[1] The polarization discontinuity in nitride heterostructures enables the formation of two-dimensional electron gases[2] (2DEGs) and 2D hole gases (2DHGs)[3] with high carrier densities. The mobility of 2DEGs at AlGaN–GaN interfaces is high and can be engineered by varying the alloy composition and barrier thickness; AlGaN/GaN HEMTs with carrier densities on the order of $\sim 10^{13}\ \text{cm}^{-2}$ are routinely achieved.[4]

The epitaxial strain in the barrier AlGaN layers grown on relaxed GaN substrates limits the composition, thickness, scaling capability, and 3D stacking for multiple channels, in addition to limiting the reliability when the devices are stressed.[5,6] Therefore, the advent of epitaxial AlInN layers that are lattice matched to GaN enabled the growth of thick barriers and even their use in Bragg reflectors photonic devices without the constraint of strain.[7] A similar advance in the last few years is of epitaxial AlScN barriers that also possess the potential for lattice-matching to GaN,[8–10] with the additional advantage of high dielectric constant[11] and potentially also ferroelectricity.[12–14] To date, the transport properties of 2DEGs formed at AlScN/GaN heterojunctions has not been investigated in detail. In this work, the transport properties of polarization-induced 2DEGs at AlScN/GaN junctions are found to be closer to that observed in AlInN/GaN junctions and both differ fundamentally from that in Al(Ga)N/GaN junctions.

AlScN/GaN HEMTs are in many ways analogous to AlInN/GaN HEMTs, which have been widely studied over the past decade. Having strong spontaneous polarization and lattice matching to GaN, AlInN enables high carrier density.[15,16] However, growing alloys of AlGaN, InGaN, AlInN, and AlScN on GaN directly leads to strong alloy scattering and, subsequently, a lower mobility.[17,18] By adding a thin AlN interlayer between the GaN channel and the AlInN barrier, AlInN/AlN/GaN HEMTs with high room-temperature electron mobility and low sheet resistance have been demonstrated.[15,19,20] Similarly, AlScN/GaN HEMTs are found to need an AlN interlayer to improve electron mobility and reduce sheet resistance.[21–23] However, low temperature electron mobility values and the physics behind electron transport in AlScN/GaN heterostructures have not been reported.

Through temperature-dependent Hall-effect measurements and modeling of electron scattering mechanisms in semiconductors, this work discusses the mobility limits in AlScN/GaN heterostructures.

AlScN/GaN and AlScN/AlN/GaN heterostructures for this study were epitaxially grown in a reactive nitrogen environment using a Veeco GenXplor MBE system. Metals (Al, Sc, and Ga) were provided from Knudsen effusion cells. Sc specifically was provided from a high temperature effusion cell. Reactive nitrogen was supplied using 200 W RF nitrogen plasma power and 1.95 sccm flow rate. Metal fluxes were characterized by measuring beam equivalent pressures (BEPs) from a beam flux monitor (BFM). Sc and Al atomic compositions were adjusted by changing the ratio of Sc and Al fluxes from effusion cells. The AlScN layers were grown under nitrogen-rich conditions with III/V ratio of 0.85 at a substrate temperature of 600 °C, measured by a thermocouple.

For each sample, a 300-nm-thick MBE GaN buffer layer was epitaxially grown under Ga-rich conditions on a semi-insulating GaN–SiC template. Two series of samples were grown to study the effect of an interlayer in the HEMT structure. The first series includes AlScN/GaN samples grown without an AlN interlayer in which the AlScN barrier was grown directly on top of GaN [Fig. 1(b)]. Excess Ga was thermally desorbed before AlScN growth to prevent Ga incorporation into AlScN. The second series consists of AlScN/AlN/GaN samples in which a thin (2 nm) interlayer of AlN was introduced between the GaN channel and the AlScN barrier [Fig. 1(a)]. The excess Ga was not thermally desorbed before the growth of the AlN interlayer growth to enhance the surface adatom mobility. The excess Ga was thermally desorbed prior to the growth of the AlScN. Finally, a 2.5 nm GaN cap layer was grown on top of the AlScN barrier [Fig. 1(a)].

Structural and morphological information were obtained from high-resolution x-ray diffraction (HR-XRD) and atomic force microscopy (AFM), respectively. The surface root mean squared (rms) roughness of AlScN/GaN samples were ∼1 nm, with features originating from threading dislocations from the GaN–SiC substrate. Room temperature and cryogenic electrical properties of the samples were investigated by a Nanometrics Hall system. Temperature-dependent characterization of electrical properties was conducted using a Lakeshore Hall system with magnetic field varied between −1 and 1 T. All Hall measurements employed the van der Pauw configuration.

Temperature-dependent Hall effect measurements were performed from 10 to 300 K using a van der Pauw geometry. Figure 1 shows the heterostructure schematics, along with their corresponding

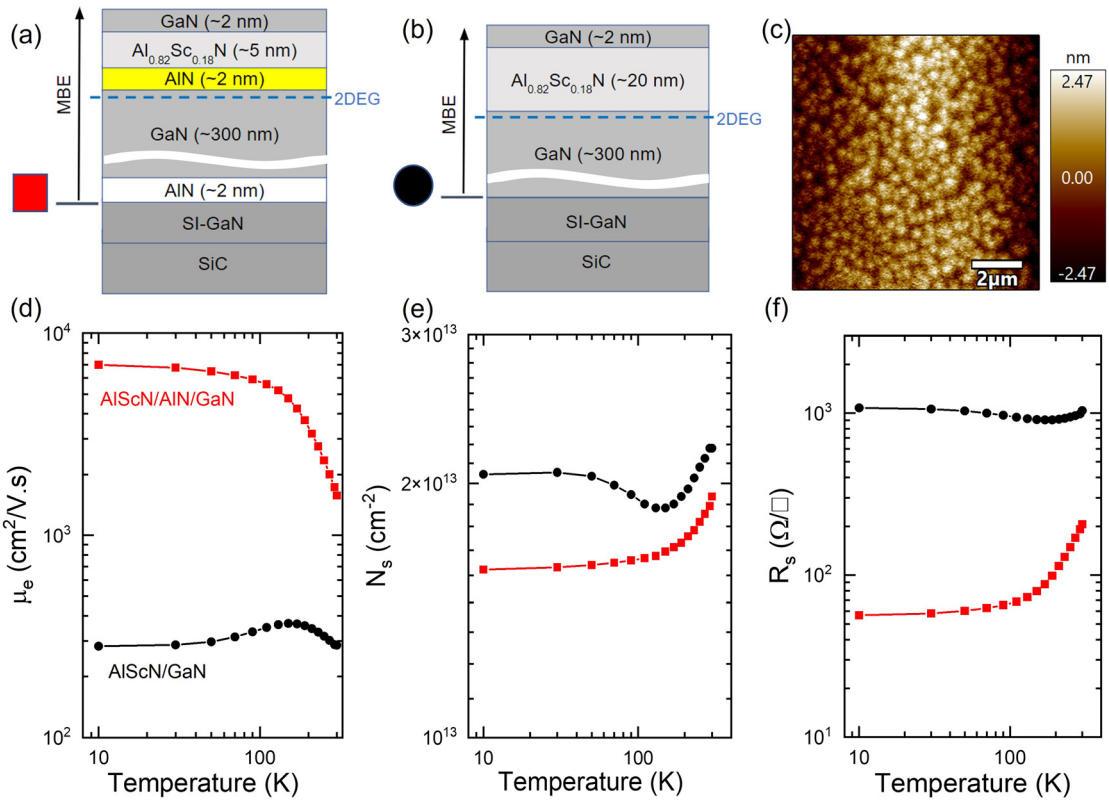

FIG. 1. (a) Schematic sample structure of AlScN/AlN/GaN series with an AlN interlayer and a thin nucleation layer. (b) Schematic sample structure of AlScN/GaN series without an AlN interlayer. (c) Representative 10×10 μm^2 AFM micrograph of the AlScN/GaN sample reported in this work; the rms roughness of this sample is 1.08 nm. Temperature-dependent (d) Hall mobility, (e) sheet carrier density, and (f) sheet resistance of AlScN/AlN/GaN and AlScN/GaN heterostructures. Using an AlN interlayer, a high electron mobility of 1573 $cm^2/V\,s$ is obtained. Without the AlN interlayer, a lower mobility of ∼300 $cm^2/V\,s$ is obtained. In the AlScN/AlN/GaN structure, electron mobility increases as a function of decreasing temperature, and the sheet carrier density is roughly constant, which is indicative of expected 2DEG electronic transport. Accordingly, the sheet resistance decreases as the temperature is lowered. In the AlScN/GaN structure, sheet carrier density, mobility and sheet resistance remain relatively constant with respect to temperature.

temperature-dependent electron mobility, sheet carrier density, and sheet resistance. Without the AlN interlayer, the Hall mobility is limited to below 300 cm^2/V s at room temperature. The carrier density and mobility in AlScN/GaN are comparable to those of Si MOSFETs. Lowering temperature does not significantly impact the Hall mobility, with the highest mobility $\mu_e = 367\ cm^2/V$ s observed at 150 K. Similarly, sheet carrier density n_s showed a weak temperature dependence, decreasing from $2.20 \times 10^{13}\ cm^{-2}$ (300 K) to $1.87 \times 10^{13}\ cm^{-2}$ (150 K) then slightly increasing to $2.05 \times 10^{13}\ cm^{-2}$ (10 K). The sheet resistance R_s varies between 906 and 1076 Ω/□. A typical 2DEG behavior would correspond to a small decrease in sheet carrier density due to minimal carrier freeze out as temperature decreases.

However, the carrier density in the AlScN/GaN sample exhibits a non-monotonic change with temperature, reaching a minimum at 150 K. This behavior could potentially be due to parallel conduction. By inserting an AlN interlayer, a small monotonic decrease in n_s from $1.93 \times 10^{13}\ cm^{-2}$ (300 K) to $1.58 \times 10^{13}\ cm^{-2}$ (10 K) corresponding to 2DEG behavior with slight carrier freeze out was observed. Drastic changes in Hall mobility and sheet resistance further corroborate the presence of a well-confined 2DEG at the AlN–GaN interface, with μ_e monotonically increasing from 1573 cm^2/V s (300 K) to 6980 cm^2/V s (10 K) and R_s decreases from 206 Ω/□ (300 K) to 57 Ω/□ (10 K). The strong temperature dependence of these transport characteristics in the sample with an AlN interlayer suggests that the electron transport is regulated by different scattering mechanisms in different temperature regimes.

Using the one-dimensional (1D) Poisson solver,[24] one-dimensional Schrödinger and Poisson equations were solved self-consistently for the energy band diagrams and electron distribution function of $Al_{0.82}Sc_{0.18}N$/GaN heterostructures with and without the AlN interlayer (Fig. 2). Using a surface Schottky barrier of 2 eV, a theoretical calculation suggests $n_s = 0.63 \times 10^{13}\ cm^{-2}$ and $n_s = 2.23 \times 10^{13}\ cm^{-2}$ for 5 nm AlScN/GaN and 5 nm AlScN/2 nm AlN/GaN heterostructures, respectively. Increasing the AlScN thickness enhances the polarization-induced 2DEG density (Fig. S1). As electron mobility is dependent on sheet density in polar nitride heterostructures, thicker AlScN barriers (10 and 20 nm) were grown without an AlN interlayer to achieve similar sheet densities between AlScN/GaN and AlScN/AlN/GaN heterostructures (Fig. S2). The 10 nm AlScN/GaN sample showed slightly lower $n_s = 1.84 \times 10^{13}\ cm^{-2}$ but higher $R_s = 1572$ Ω/□ and lower $\mu_e = 215\ cm^2/V$ s (300 K). Thus, the 20 nm AlScN/GaN sample was compared with the AlScN/AlN/GaN sample to best illustrate the effect of the AlN interlayer (Fig. 1). The experimental sheet densities are lower than predicted values, likely due to the fewer surface states being ionized at the GaN cap.[25] Owing to the high conduction band offset between GaN and $Al_{0.82}Sc_{0.18}N$,[26] electron wavefunction penetration into the AlScN barrier is not significant. However, this penetration can be nearly eliminated by introducing a thin AlN interlayer. Although electrons in AlN have a higher effective mass than GaN, less than one percent of electrons penetrate into the AlN interlayer. The AlN interlayer helps minimize effects of alloy scattering between the $Al_{0.82}Sc_{0.18}N$ barrier and the GaN channel. Another effect of the AlN interlayer is the enhanced carrier confinement. Due to a shallower potential well at the AlScN–GaN interface, the electron wavefunction is more loosely confined when an AlN interlayer is not used (Fig. 2). Thus, the positive impact of AlN observed experimentally is corroborated by simulations.

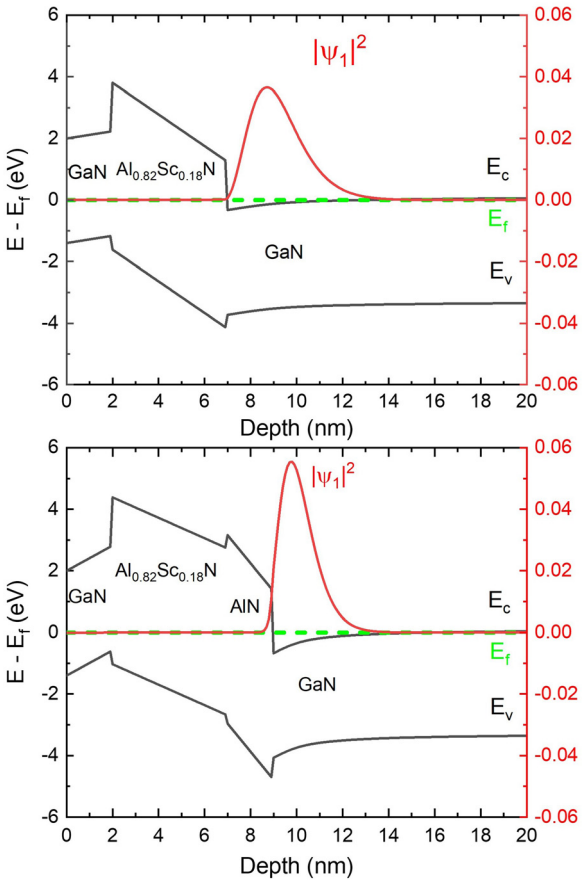

FIG. 2. 1D Poisson equilibrium band diagram of (a) AlScN/GaN and (b) AlScN/AlN/GaN heterostructures. The square of the highest occupied energy level of the electron wavefunction in the 2DEG is shown in both heterostructures. AlN serves an interlayer to enhance electron wavefunction confinement and block electron wavefunction penetration into the AlScN barrier. Electric field profile changes across the AlScN–AlN interface because AlScN is a high-κ dielectric material.[11]

Figure 3 summarizes transport properties of AlScN/AlN/GaN heterostructures. At 206 Ω/□, the AlScN/AlN/GaN structure discussed in this work achieves one of the lowest room temperature sheet resistances reported to date. Although higher mobility and high carrier density AlN/GaN structures have been reported in the past,[27–30] AlN suffers from a low critical thickness (e.g., 6–7 nm) due to the lattice mismatch and accompanying tensile strain between AlN and GaN when grown on relaxed GaN layers.[9,27] On the other hand, AlScN can be lattice-matched to relaxed GaN, which allows for enhanced tunability in both the sheet carrier density and barrier layer thickness. In addition, the enhanced relative dielectric permittivity of AlScN is attractive for device scaling.[11] The electron mobility of 6094 cm^2/V s at 77 K and 6980 cm^2/V s at 10 K for the AlScN/AlN/GaN heterostructure are the highest values reported to date for scandium containing nitride epitaxial heterostructures.

The temperature-dependent Hall mobilities are compared to a theoretical model to explore the dominant scattering mechanisms.[33] The model includes intrinsic scattering mechanisms from polar optical

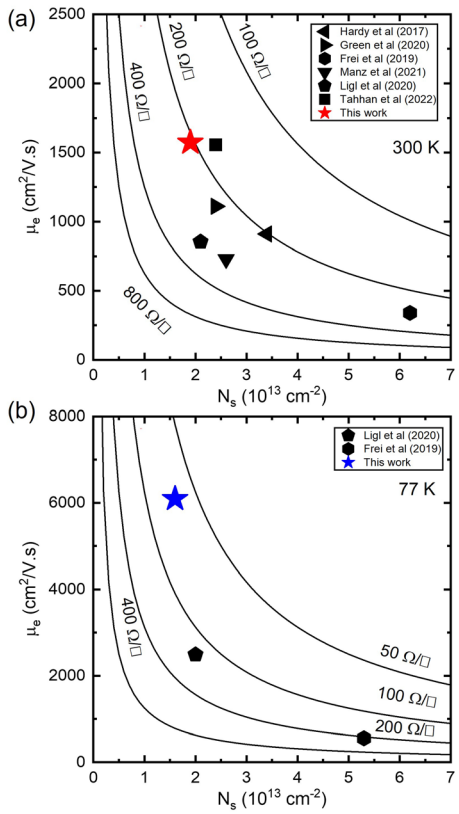

FIG. 3. Comparison of electron mobilities for various AlScN–AlN–GaN 2DEGs as a function of sheet carrier density at (a) 300 and (b) 77 K. Constant sheet resistance contour plots are shown.[8,10,22,23,31,32]

phonons (POP), acoustic phonons due to deformation potential, and piezoelectric (PZ) scattering. The model also includes extrinsic scattering mechanisms such as ionized impurity, dislocation, alloy disorder, and interface roughness (IR). The parameters used in these calculations are shown in Table I. The theoretical mobility obtained from this model is compared with the experimental Hall mobility of the AlScN/AlN/GaN sample (Fig. 4).

The intrinsic scattering mechanism due to polar optical phonons dominates the transport characteristics at temperatures above 200 K. The experimental mobility measured near room temperature is higher than the theoretically estimated mobility for the polar optical phonon limit (Fig. 4). A similar effect is observed in high quality AlN/GaN HEMT heterostructures, where experimental mobility slightly exceeds the phonon-limited mobility predicted by theoretical models.[30] If extrinsic scattering mechanisms are not dominant, Hall mobility should drastically increase at low temperature to follow the phonon-limited mobility values.

From the theoretical model, electron mobility at low temperatures is regulated by a combination of acoustic phonon scattering and a temperature-independent extrinsic mechanism. By adding an AlN interlayer, alloy disorder scattering is suppressed and is not the limiting factor of low-temperature Hall mobility. Dislocation scattering and ionized impurity scattering also do not have noticeable effects on the

TABLE I. Summary of constants used and results extracted from the calculation of scattering mechanisms in AlScN/AlN/GaN.

Quantity[a]	Value (unit)
Lattice constant (GaN), a_0	3.189 (Å)
Lattice constant (GaN), c_0	5.185 (Å)
Relative dielectric constant (GaN), ε_r	8.9 (ε_0)
LO phonon energy	92 (meV)
Effective mass in GaN, m^*	0.22 (m_0)
Effective mass in $Al_{0.82}Sc_{0.18}N$,[b] m_b^*	0.46 (m_0)
Alloy scattering potential, V_0	1.8 (eV)
Acoustic deformation potential	8.3 (eV)
Conduction band offset,[c] ΔE_c	2.0 (eV)
Thickness variation, δ	5.185 (Å)
Correlation length, λ	41.457 (Å)

[a]Parameters affecting theoretical modeling of scattering mechanisms.[33]
[b]Calculated electron effective mass in $Al_{0.82}Sc_{0.18}N$.[37]
[c]Conduction band offset between $Al_{0.82}Sc_{0.18}N$ and GaN.[26]

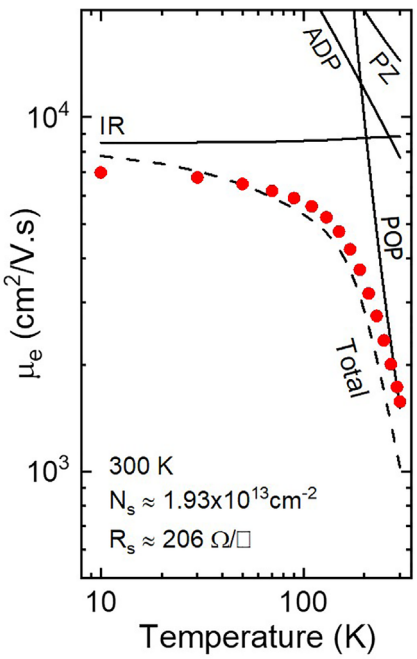

FIG. 4. Overlaid electron mobility limiting mechanisms with temperature-dependent Hall effect data (red circles). Matthiessen's rule was utilized to calculate a total mobility (dashed line) from contributing scattering mechanisms. Acoustic deformation (ADP) and piezoelectric (PZ) phonon scatterings weakly limit mobility near room temperature. At room temperature, the electron mobility is limited by an intrinsic scattering mechanism: polar optical phonons (POP). Accordingly, changes in growth conditions will not improve the electron mobility. At low temperatures, the electron mobility is limited by an extrinsic scattering mechanism: interface roughness scattering (IR). Here, changes in growth conditions can improve the electron mobility. The effects of ionized impurity, dislocation and alloy disorder scatterings are negligible given the parameters used in the model.

Hall mobility for dislocation density up to $5 \times 10^{10}\,\mathrm{cm}^{-2}$ and ionized impurity density up to $10^{18}\,\mathrm{cm}^{-3}$. Instead, interface roughness scattering limits the electron mobility at low temperature, as shown in Fig. 4. Interface roughness scattering can be characterized by two parameters: thickness variation (δ) and correlation length (λ). A rougher interface corresponds to a higher δ and a shorter λ. It is important to note that δ and λ are dependent on each other and a more general indicator of interface quality is the λ/δ ratio. Studies on transport characteristics of AlGaN/GaN HEMT heterostructures have reported λ/δ ratio between 5 and 10.[19,34–36] For a high quality growth, the vertical thickness variation δ varies between one and three monolayers and can be correlated with rms roughness. In this work, δ was chosen to be the length along c-axis of a GaN unit cell ($\delta = 5.185$ Å), or two monolayers. This value is close to the measured rms roughness obtained from atomic force microscopy images. By fitting the theoretical model to experimental data, $\delta = 5.185$ Å and $\lambda = 41.457$ Å were estimated (Table I). The ratio $\lambda/\delta \approx 8$ agrees well with reported values in high quality AlGaN/GaN heterostructures.[19,34,36]

Experimentally, there is a stark difference between electron mobilities of samples with and without the AlN interlayer at low temperature [Fig. 1(d)]. Electron mobility of the AlScN/GaN sample remains relatively constant with respect to temperature, suggesting a combination of temperature-independent, extrinsic scattering mechanisms at play. Based on similar rms roughness values obtained from AFM analysis, interface roughness scattering does not change significantly between samples. As previously discussed, extrinsic scattering mechanisms such as ionized impurity scattering and dislocation scattering do not have a significant impact on carrier mobility at the levels of impurity and dislocation density expected in these samples. Therefore, the drop in mobility in AlScN/GaN sample could be due to alloy scattering. The effect of alloy scattering at the AlScN–GaN interface on 2D electron mobility is given by

$$\mu_{alloy}^{2d} = \frac{q\hbar^3}{(m^*)^2 \Omega_0 V_0^2 x(1-x)} \frac{2}{\kappa_b P_b^2}, \tag{1}$$

where q is the electron charge, $\hbar$ is the reduced Planck constant, $m^* = 0.22m_0$ is the effective mass of electron in the GaN channel, $\Omega_0 = \left(\sqrt{3}/8\right)a_0^2 c_0$ is the scattering volume, V_0 is the alloy scattering potential, x is the Sc composition, and $\kappa_b = 2\sqrt{(2m_b^*\Delta E_c)/\hbar^2}$ is the inverse penetration depth of electrons into the alloy barrier and is dependent on the conduction band offset ΔE_c and the effective mass of electron in the alloy barrier m_b^*. The penetration probability P_b of electrons into the alloy barrier is given by

$$P_b = \frac{2b^3}{\left(b + \kappa_b \frac{m^*}{m_b}\right)^2 + 2b\left(b + \kappa_b \frac{m^*}{m_b}\right) + 2b^2\left(1 + \frac{b}{\kappa_b}\right)}, \tag{2}$$

where $b = [(33m^* q^2 n_{2d})/(8\varepsilon_s \hbar^2)]^{1/3}$ is the variational Fang–Howard wavefunction parameter that quantifies the spatial spread of the 2DEG, and $\varepsilon_s = 8.9\varepsilon_0$ is the static permittivity of GaN.[33]

Using $\Delta E_c = 2.0$ eV and $m_b^* = 0.46m_0$ for $Al_{0.82}Sc_{0.18}N$,[26,37] an unreasonably high scattering potential of $V_0 \approx 50$ eV would be necessary explain $\mu_e \approx 300$ $\mathrm{cm}^2/\mathrm{V\ s}$ observed in AlScN/GaN sample. Because the alloy scattering potential is limited by band offsets of semiconductors, it should be much smaller. For comparison, scattering potentials reported in AlGaN and InGaN are between 1.3 and 2.3 eV.[17,38,39] The extreme alloy scattering potential needed to match the current experimental results suggests a limitation of the theoretical model.

Fermi's Golden Rule is used to derive the alloy scattering rate results mentioned earlier. Different than AlN and GaN, and their alloys where the conduction band is dominated by s-orbital character, the localized nature of the d-orbitals of Sc atoms in AlScN could generate a strong conduction band perturbation, resulting in stronger alloy scattering effect that would violate the Fermi Golden Rule and Born approximation. In addition, the bandgap mismatch in AlScN between the constituent binaries AlN and ScN is much larger than AlN/GaN or even GaN/InN. They are similar to the bandgap difference between AlN and InN, and it is interesting to observe that the mobilities of AlScN/GaN 2DEGs are similar to those in InAlN/GaN 2DEGs without the AlN interlayers. The effect of higher order scattering events beyond the Born approximation has been observed in and discussed for dilute nitride semiconductors. In such mismatched alloys, the conduction band perturbation was incorporated to help explain why experimental mobilities are substantially lower than predicted by Born approximation and weak alloy scattering.[40] A future study adapting alloy scattering models for the scattering of electrons due to conduction band perturbation is needed to elucidate the 2DEG mobility limit observed in AlScN/GaN 2DEGs in this work.

In conclusion, temperature-dependent transport properties of MBE AlScN/GaN HEMT heterostructures were performed down to 10 K, revealing the underlying scattering mechanisms that affect the electron mobility in AlScN/GaN heterostructures. At high temperatures, transport properties of AlScN/GaN HEMT heterostructures are intrinsically limited by polar and acoustic phonon scattering. In the absence of an AlN interlayer, AlScN/GaN heterostructures suffer from strong alloy and interface roughness scattering. By introducing an AlN interlayer, alloy scattering is minimized, as demonstrated by theoretical simulation and experimental data. In AlScN/AlN/GaN samples, transport properties are dominated by interface roughness scattering at low temperature. The use of Ga droplets as a wetting method alleviates effects of interface roughness scattering, yielding a room temperature mobility of $1573\,\mathrm{cm}^2/\mathrm{V\ s}$ and sheet resistance of 206 Ω/□ at a sheet carrier density of $1.93 \times 10^{13}\,\mathrm{cm}^{-2}$. A record high electron mobility of 6980 and $6094\,\mathrm{cm}^2/\mathrm{V\ s}$ and a record low sheet resistance of 57 and 63 Ω/□ were also measured at 10 and 77 K, respectively. AlScN/AlN/GaN heterostructures grown by MBE demonstrate similar transport properties to some of the best reported AlN/GaN heterostructures. More importantly, the strong piezoelectric and spontaneous polarization provided by AlScN enables tunable carrier density in GaN-based 2DEGs, especially in the high carrier density regime ($>3 \times 10^{13}\,\mathrm{cm}^{-2}$). The ability to achieve high mobility and high carrier density in AlScN/GaN HEMT heterostructures and to understand the mechanisms that limit electron mobility allows for the merging of the promising physical properties of epitaxial AlScN with nitride semiconductors.

See the supplementary material for a comparison of predicted and measured sheet carrier densities and for further electrical transport data on AlScN/GaN HEMT heterostructures.

This work was supported, in part, by Northrop Grumman Mission Systems university research funding. This work was

supported, in part, by the DARPA Tunable Ferroelectric Nitrides (TUFEN) program monitored by Dr. Ronald G. Polcawich and Dr. Ali Kezhavarzi. This work was supported in part by a DARPA-Sponsored Special Project (DSSP), monitored by Dr. Thomas Kazior. This work was supported, in part, by the AFOSR (Grant No. FA9550-20-1-0148, Program Officer: Dr. Kenneth Goretta). This work was performed in part at the Cornell NanoScale Facility, a member of the National Nanotechnology Coordinated Infrastructure (NNCI), which is supported by the National Science Foundation (Grant No. NNCI-2025233). This work made use of the Cornell Center for Materials Research Shared Facilities, which are supported through the NSF MRSEC program (No. DMR-1719875). The authors would like to acknowledge the Materials Preparation Center, Ames Laboratory, U.S. DOE Basic Energy Sciences, Ames, IA, USA for supplying the Sc source material.

AUTHOR DECLARATIONS

Conflict of Interest

The authors have no conflicts to disclose.

Author Contributions

Joseph Casamento and Thai-Son Nguyen contributed equally to this work.

Joseph Casamento: Conceptualization (lead); Data curation (equal); Formal analysis (equal); Investigation (equal); Methodology (equal); Resources (equal); Software (supporting); Writing – original draft (equal); Writing – review & editing (equal). **Thai-Son Nguyen:** Data curation (equal); Formal analysis (equal); Investigation (equal); Methodology (equal); Software (lead); Writing – original draft (equal); Writing – review & editing (equal). **YongJin Cho:** Data curation (supporting); Investigation (supporting); Methodology (supporting). **Chandrashekhar Prakash Savant:** Data curation (supporting); Investigation (supporting); Methodology (supporting). **Tim Vasen:** Funding acquisition (lead); Investigation (supporting); Project administration (lead); Resources (lead); Writing – review & editing (supporting). **Shamima Afroz:** Investigation (supporting); Project administration (supporting); Resources (supporting); Writing – review & editing (supporting). **Daniel J. Hannan:** Investigation (equal); Project administration (supporting); Resources (supporting); Writing – review & editing (supporting). **Huili Grace Xing:** Conceptualization (supporting); Investigation (equal); Project administration (equal); Supervision (supporting); Writing – original draft (supporting); Writing – review & editing (supporting). **Debdeep Jena:** Conceptualization (supporting); Investigation (supporting); Methodology (supporting); Project administration (equal); Supervision (lead); Writing – original draft (supporting); Writing – review & editing (supporting).

DATA AVAILABILITY

The data that support the findings of this study are available from the corresponding author upon reasonable request.

REFERENCES

[1]R. Vetury, N. Q. Zhang, S. Keller, and U. K. Mishra, "The impact of surface states on the DC and RF characteristics of AlGaN/GaN HFETs," IEEE Trans. Electron Devices **48**, 560–566 (2001).
[2]O. Ambacher, J. Smart, J. Shealy, N. Weimann, K. Chu, M. Murphy, W. Schaff, L. Eastman, R. Dimitrov, L. Wittmer *et al.*, "Two-dimensional electron gases induced by spontaneous and piezoelectric polarization charges in N-and Ga-face AlGaN/GaN heterostructures," J. Appl. Phys. **85**, 3222–3233 (1999).
[3]R. Chaudhuri, S. J. Bader, Z. Chen, D. A. Muller, H. G. Xing, and D. Jena, "A polarization-induced 2D hole gas in undoped gallium nitride quantum wells," Science **365**, 1454–1457 (2019).
[4]Y. Cho, Y. Ren, H. G. Xing, and D. Jena, "High-mobility two-dimensional electron gases at AlGaN/GaN heterostructures grown on GaN bulk wafers and GaN template substrates," Appl. Phys. Express **12**, 121003 (2019).
[5]M. Kuball, M. Ťapajna, R. J. Simms, M. Faqir, and U. K. Mishra, "AlGaN/GaN HEMT device reliability and degradation evolution: Importance of diffusion processes," Microelectron. Reliab. **51**, 195–200 (2011).
[6]J. A. del Alamo and J. Joh, "GaN HEMT reliability," Microelectron. Reliab. **49**, 1200–1206 (2009).
[7]J.-F. Carlin, C. Zellweger, J. Dorsaz, S. Nicolay, G. Christmann, E. Feltin, R. Butté, and N. Grandjean, "Progresses in III-nitride distributed Bragg reflectors and microcavities using AlInN/GaN materials," Phys. Status Solidi B **242**, 2326–2344 (2005).
[8]M. T. Hardy, B. P. Downey, N. Nepal, D. F. Storm, D. S. Katzer, and D. J. Meyer, "Epitaxial ScAlN grown by molecular beam epitaxy on GaN and SiC substrates," Appl. Phys. Lett. **110**, 162104 (2017).
[9]T. E. Kazior, E. M. Chumbes, B. Schultz, J. Logan, D. J. Meyer, and M. T. Hardy, "High power density ScAlN-based heterostructure FETs for mm-wave applications," in *IEEE MTT-S International Microwave Symposium (IMS)* (IEEE, 2019), pp. 1136–1139.
[10]J. Ligl, S. Leone, C. Manz, L. Kirste, P. Doering, T. Fuchs, M. Prescher, and O. Ambacher, "Metalorganic chemical vapor phase deposition of AlScN/GaN heterostructures," J. Appl. Phys. **127**, 195704 (2020).
[11]J. Casamento, H. Lee, T. Maeda, V. Gund, K. Nomoto, L. van Deurzen, W. Turner, P. Fay, S. Mu, C. Van de Walle, A. Lal, H. Xing, and D. Jena, "Epitaxial $Sc_xAl_{1-x}N$ on GaN is a high K dielectric," Appl. Phys. Lett. **120**, 152901 (2022).
[12]P. Wang, D. Wang, N. M. Vu, T. Chiang, J. T. Heron, and Z. Mi, "Fully epitaxial ferroelectric ScAlN grown by molecular beam epitaxy," Appl. Phys. Lett. **118**, 223504 (2021).
[13]D. Wang, P. Wang, S. Mondal, S. Mohanty, T. Ma, E. Ahmadi, and Z. Mi, "An epitaxial ferroelectric ScAlN/GaN heterostructure memory," Adv. Electron. Mater. **8**, 2200005 (2022).
[14]J. Casamento, V. Gund, H. Lee, K. Nomoto, T. Maeda, B. Davaji, M. J. Asadi, J. Wright, Y.-T. Shao, D. A. Muller, A. Lal, X. Huili, and D. Jena, "Ferroelectricity in polar ScAlN/GaN epitaxial semiconductor heterostructures," arXiv:org:abs/2105.10114 (2021).
[15]M. Gonschorek, J.-F. Carlin, E. Feltin, M. Py, and N. Grandjean, "High electron mobility lattice-matched AlInN/GaN field-effect transistor heterostructures," Appl. Phys. Lett. **89**, 062106 (2006).
[16]F. Medjdoub, J.-F. Carlin, M. Gonschorek, E. Feltin, M. Py, D. Ducatteau, C. Gaquiere, N. Grandjean, and E. Kohn, "Can InAlN/GaN be an alternative to high power/high temperature AlGaN/GaN devices?," in *International Electron Devices Meeting* (IEEE, 2006), pp. 1–4.
[17]E. Bellotti, F. Bertazzi, and M. Goano, "Alloy scattering in AlGaN and InGaN: A numerical study," J. Appl. Phys. **101**, 123706 (2007).
[18]Y. Li, J. Zhang, W. Wan, Y. Zhang, Y. Nie, J. Zhang, and Y. Hao, "Alloy disorder scattering limited mobility of two-dimensional electron gas in the quaternary AlInGaN/GaN heterojunctions," Physica E **67**, 77–83 (2015).
[19]A. Teke, S. Gökden, R. Tülek, J. Leach, Q. Fan, J. Xie, Ü. Özgür, H. Morkoç, S. Lisesivdin, and E. Özbay, "The effect of AlN interlayer thicknesses on scattering processes in lattice-matched AlInN/GaN two-dimensional electron gas heterostructures," New J. Phys. **11**, 063031 (2009).
[20]S. W. Kaun, E. Ahmadi, B. Mazumder, F. Wu, E. C. Kyle, P. G. Burke, U. K. Mishra, and J. S. Speck, "GaN-based high-electron-mobility transistor structures with homogeneous lattice-matched InAlN barriers grown by plasma-assisted molecular beam epitaxy," Semicond. Sci. Technol. **29**, 045011 (2014).
[21]A. J. Green, J. K. Gillespie, R. C. Fitch, D. E. Walker, M. Lindquist, A. Crespo, D. Brooks, E. Beam, A. Xie, V. Kumar *et al.*, "ScAlN/GaN high-electron-mobility transistors with 2.4-A/mm current density and 0.67-S/mm transconductance," IEEE Electron Device Lett. **40**, 1056–1059 (2019).

[22]A. J. Green, N. Moser, N. C. Miller, K. J. Liddy, M. Lindquist, M. Elliot, J. K. Gillespie, R. C. Fitch, R. Gilbert, D. E. Walker *et al.*, "RF power performance of Sc(Al, Ga)N/GaN HEMTs at Ka-band," IEEE Electron Device Lett. **41**, 1181–1184 (2020).
[23]C. Manz, S. Leone, L. Kirste, J. Ligl, K. Frei, T. Fuchs, M. Prescher, P. Waltereit, M. A. Verheijen, A. Graff *et al.*, "Improved AlScN/GaN heterostructures grown by metal-organic chemical vapor deposition," Semicond. Sci. Technol. **36**, 034003 (2021).
[24]See G. Snider, https://www3.nd.edu/gsnider/ for "1D Poisson Solver."
[25]B. Jogai, "Influence of surface states on the two-dimensional electron gas in AlGaN/GaN heterojunction field-effect transistors," J. Appl. Phys. **93**, 1631–1635 (2003).
[26]E. N. Jin, M. T. Hardy, A. L. Mock, J. L. Lyons, A. R. Kramer, M. J. Tadjer, N. Nepal, D. S. Katzer, and D. J. Meyer, "Band alignment of $Sc_xAl_{1-x}N$/GaN heterojunctions," ACS Appl. Mater. Interfaces **12**, 52192–52200 (2020).
[27]Y. Cao and D. Jena, "High-mobility window for two-dimensional electron gases at ultrathin AlN/GaN heterojunctions," Appl. Phys. Lett. **90**, 182112 (2007).
[28]Y. Cao, K. Wang, G. Li, T. Kosel, H. Xing, and D. Jena, "MBE growth of high conductivity single and multiple AlN/GaN heterojunctions," J. Cryst. Growth **323**, 529–533 (2011).
[29]A. Dabiran, A. Wowchak, A. Osinsky, J. Xie, B. Hertog, B. Cui, D. C. Look, and P. Chow, "Very high channel conductivity in low-defect AlN/GaN high electron mobility transistor structures," Appl. Phys. Lett. **93**, 082111 (2008).
[30]Y. Cao, K. Wang, and D. Jena, "Electron transport properties of low sheet-resistance two-dimensional electron gases in ultrathin AlN/GaN heterojunctions grown by MBE," Phys. Status Solidi C **5**, 1873–1875 (2008).
[31]K. Frei, R. Trejo-Hernández, S. Schütt, L. Kirste, M. Prescher, R. Aidam, S. Müller, P. Waltereit, O. Ambacher, and M. Fiederle, "Investigation of growth parameters for ScAlN-barrier HEMT structures by plasma-assisted MBE," Jpn. J. Appl. Phys., Part 1 **58**, SC1045 (2019).
[32]M. B. Tahhan, J. A. Logan, M. T. Hardy, M. G. Ancona, B. Schultz, B. Appleton, T. Kazior, D. J. Meyer, and E. M. Chumbes, "Passivation schemes for ScAlN-barrier mm-wave high electron mobility transistors," IEEE Trans. Electron Devices **69**, 962–967 (2022).
[33]D. Jena, *Quantum Physics of Semiconductor Materials and Devices* (Oxford University Press, 2022).
[34]D. Zanato, S. Gokden, N. Balkan, B. Ridley, and W. J. Schaff, "The effect of interface-roughness and dislocation scattering on low temperature mobility of 2D electron gas in GaN/AlGaN," Semicond. Sci. Technol. **19**, 427 (2004).
[35]S. Gökden, R. Baran, N. Balkan, and S. Mazzucato, "The effect of interface roughness scattering on low field mobility of 2D electron gas in GaN/AlGaN heterostructure," Physica E **24**, 249–256 (2004).
[36]M. K. Mishra, R. K. Sharma, R. Manchanda, R. K. Bag, O. P. Thakur, and R. Muralidharan, "Comprehensive magnetotransport characterization of two dimensional electron gas in AlGaN/GaN high electron mobility transistor structures leading to the assessment of interface roughness," AIP Adv. **4**, 097124 (2014).
[37]H. Fu, J. C. Goodrich, O. Ogidi-Ekoko, and N. Tansu, "Power electronics figure-of-merit of ScAlN," Appl. Phys. Lett. **119**, 072101 (2021).
[38]D. Jena, S. Heikman, J. S. Speck, A. Gossard, U. K. Mishra, A. Link, and O. Ambacher, "Magnetotransport properties of a polarization-doped three-dimensional electron slab in graded AlGaN," Phys. Rev. B **67**, 153306 (2003).
[39]J. Simon, A. Wang, H. Xing, S. Rajan, and D. Jena, "Carrier transport and confinement in polarization-induced three-dimensional electron slabs: Importance of alloy scattering in AlGaN," Appl. Phys. Lett. **88**, 042109 (2006).
[40]S. Fahy and E. P. O'Reilly, "Intrinsic limits on electron mobility in dilute nitride semiconductors," Appl. Phys. Lett. **83**, 3731–3733 (2003).